Friction Hysteresis Modeling and Force Control in a Constrained Single-link Arm[1]

A. Bazaei
School of Electrical Engineering
and Computer Science,
University of Newcastle,
NSW 2308, Australia
e-mail: Ali.Bazaei@newcastle.edu.au

M. Moallem[2]
Mechatronics Systems Engineering,
School of Engineering Science,
Simon Fraser University,
Surrey, BC, V3T 0A3, Canada
e-mail: mmoallem@sfu.ca

In this paper, we study friction characteristics of a constrained planar single-link arm in applications, where control of the end-point interaction force is required. The objective is to improve performance of a force control system by developing an adequate friction model. It is shown that hub friction increases with the applied force with the end-point force exhibiting significant hysteresis behavior. A friction model is presented for capturing these phenomena and compared with the widely used LuGre friction model. Effectiveness of the proposed model for friction compensation is further examined on an experimental force control system testbed. [DOI: 10.1115/1.4004580]

Keywords: friction model, hysteresis behavior, force control, friction compensation

1 Introduction

Friction is an inevitable phenomenon which exists in almost all mechanical systems. Although it may be helpful in certain cases due to its energy dissipative nature, it can deteriorate precise control performance as a result of its nonlinear, time-varying, and random characteristics. Knowledge of friction behavior in a particular control system would lead to a better controller design and hence better system performance [1].

Research on friction started from 14th century by Leonardo da Vinci and is still under progress [1–3]. As the relative velocity between two lubricated surfaces in contact increases from zero, the friction behavior undergoes four different regimes known as static friction (presliding displacement or stiction), boundary lubrication, partial fluid lubrication, and full fluid lubrication, respectively [1]. In the static friction regime, an elastic deformation, known as "microslip breakaway displacements" [4], occurs due to asperity junctions. In the second regime, which occurs at very low speeds, the surfaces slide over their thin boundary layers. In the third and fourth regimes, the velocity is enough to draw the lubricant into the contact zone, resulting in the surfaces sliding partially and completely over a layer of the lubricant, respectively.

Because the exact mechanism of friction is not well known due to the effects such as irregularity of the surfaces in contact, contaminations, unknown material properties, and immeasurability of microslip displacements in many practical situations, construction of a general friction model from physical first principles is not possible [3,5]. However, the overall behavior of friction has been approximated by static or dynamic models based on experimental observations. The static models, such as Karnopp model [6] or Armstrong-Hélouvry's model [1], do not increase the system order, but the dynamic friction models, such as Dahl model [7,8], bristle and reset integrator [9], Bliman and Sorine [10–12], lubricated contacts [13,14], LuGre [15], elasto-plastic [16,17], Leuven [18,19], and Maxwell [20,21], add extra state variables to the system.

This paper addresses the friction behavior when a robot arm is interacting with an almost stationary and rigid environment. In this case, since the angular velocity is very low, most of the time the velocity-based friction models are not suitable for prediction of the system response [22]. The torque-based friction model introduced in Ref. [22–24] was found to be useful in modeling and force control as well as in friction compensation of haptic-interfaces [25]. However, variation of the breakaway point with end-point force and hysteresis behavior of friction, which were observed experimentally in this paper, have not been investigated in existing literature.

In this paper, using the experimental setup shown in Fig. 1(*a*), which consists of a planar single-link arm driven by a current-controlled dc motor and constrained by a force sensor, we demonstrate the behavior of hub friction with applied force including its hysteresis characteristic. After combining the force sensor's mass with the arm, effect of force sensor can be modeled by a spring, as shown in the free body diagram in Fig. 1(*b*). The friction torque in this setup is mainly between the stationary part of the motor and its shaft, which is rigidly attached to the arm. The friction phenomena studied in this simple setup appears in many mechanical systems such as the usually *low speed* haptic devices. Based on the experimental studies, we construct a friction model that captures the force dependency of hub friction as well as hysteresis characteristics for a low-speed interacting arm. The model is then used for friction compensation in a precision force control feedback loop. The experimental results are presented that confirm analytical and simulation studies presented in this paper.

2 Problem Statement

Since the constrained beam is almost stationary, a permanent magnet dC motor was selected, which is suitable to apply high stall torques for long-duty cycle applications. Since the torque applied by a dC motor is linearly proportional to its armature current, a voltage to current converter was used to supply the motor current and ensure that the torque is proportional to the input command.

The experimental data shown in Fig. 2 illustrate the end-point force response of the link to a slowly varying input waveform. The angular displacements are so small that they cannot be detected by the encoder used (with resolution of 0.072 deg). The reaction end-point force F, which is measured by the force sensor, is proportional to angular displacement θ. Hence, variations of the end-point force indicate nonzero deflection of force sensor and angular displacement. Let us define major rising or falling modes by the intervals, in which the end-point force starts following the

[1]This research was supported by the Natural Sciences and Engineering Research Council (NSERC) of Canada.
[2]Corresponding author.
Contributed by the Dynamic Systems Division of ASME for publication in the Journal of Dynamic Systems, Measurement and Control. Manuscript received August 29, 2008; final manuscript received April 21, 2011; published online November 21, 2011. Assoc. Editor: Marcelo Dapino.

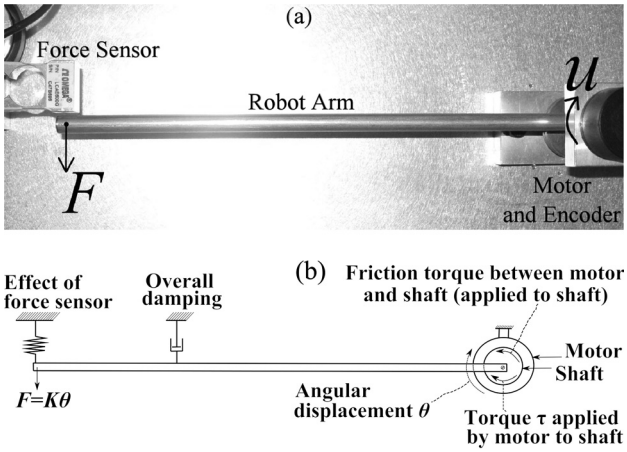

Fig. 1 (*a*) Demonstration of the planar single-link arm and (*b*) free body diagram

input with the maximum speed, as shown in Fig. 2. In such intervals, the speed is nonzero, and the friction force is equal to its threshold value, denoted by F_c^+ and $-F_c^-$ in positive and negative directions, respectively. Unconstrained tests on the setup in Fig. 1 were performed when the force sensor is removed to let the arm rotate freely. These tests indicate the unsymmetrical behavior of friction in the opposite directions, practically no motions with speeds less than 0.4 deg s^{-1}, and negligible difference between the breakaway value of friction and its kinetic value [26]. The angular speed in Fig. 2 is also much less than 0.4 deg/s[3]. Hence, different symbols F_c^+ and $-F_c^-$ are used as threshold values to represent the maximum value of friction in each direction with no distinction between the kinetic friction and the maximum value of friction in the static regime. In such a slowly varying input mode, the momentum and the acceleration are negligible and the following relationship is valid:

$$u = F + f \tag{1}$$

where u is the manipulated control input, which is proportional to the torque τ applied by the motor, and f describes the friction effect. Using the measured data in the first rising and the last falling periods of the input shown in Fig. 2, the maximum and the minimum steady-state achievable end-point forces in terms of the control input are as shown in Fig. 3(*a*). Notice that the control input signal u was scaled such that its steady-state magnitude is the same as that of the end-point force F in the absence of hub friction. To do this, we neglected gravity effects and assumed the same breakaway levels and kinetic friction magnitudes in positive and negative directions. Moreover, a constant gain was incorporated in series with the input command u to scale it appropriately. The gain was then tuned such that the graphs of the scaled input u versus the end-point force F during rising and falling periods have almost equal vertical distances from a hypothetical 45 deg line of $u = F$, as shown in Fig. 3(*a*). During major rising and falling modes, f is equal to F_c^+ and $-F_c^-$, respectively. Hence, we can approximate the expression $F_c^+ + F_c^-$ by Δu as defined in Fig. 3(*a*). The relationship $\Delta u = F_c^+ + F_c^-$ is valid even if the magnitudes of friction thresholds in opposite directions differ (i.e., $F_c^+ \neq F_c^-$), or a nonzero gravity term g exists due to a slight deviation of the rotation axis from the vertical direction, which changes Eq. (1) to $u = F + f - g$. Notice that the friction force interval $F_c^+ + F_c^-$ increases considerably with the end-point force as shown in Fig. 3(*b*). Hence, threshold values of friction, denoted by F_c^+ and $-F_c^-$, are highly dependent on the end-point force F. Thus, the hub friction increases with the force applied to the end-point. Modeling of this force-dependent friction phenomenon, which can be interpreted by the increase of the longitudinal and lateral forces at the hub as the end-point force rises, is investigated in this paper.

Another friction effect studied in this paper is the hysteresis characteristic. The kind of hysteresis considered here is different from the usual backlash-wise hysteresis between the input and the end-force, which result from multivalued nature of static friction. Considering the force dependencies of friction threshold values and the applied input in Fig. 2, traditional understanding of friction behavior implies that the end-point force should experience sharp breaks similar to the dotted line in Fig. 2[4]. The hysteresis phenomenon that we consider can cause considerable deviation of the end-point force from typical values predicted by traditional friction models as shown in Fig. 2. This deviation will be more significant when the net external force $u - F$ is highly in the opposite direction of its oncoming values. This phenomenon is illustrated in Fig. 2 which is described as follows. Consider any time interval during which the control input changes monotonically. At the beginning of each time interval, the end-point force F is almost constant and at the end of each interval, F experiences a major falling or rising mode if the time duration and input rate are large enough for the net-force to overcome the breakaway level. In the intervals marked by "Gradual Transitions," the transition of end-point force from the almost constant mode to the major falling or rising mode happens gradually. However, there are special situations where the transition from constant to major mode occurs almost sharply rather than gradually, as indicated by "Almost Sharp Transition" ($33.5\ \text{s} < t < 38\ \text{s}$ in Fig. 2). Referring to this figure, increasing control input u results in an almost sharp transition of F to a major rising mode when u is large enough to overcome the breakaway level, e.g., at $t = 38$ s in Fig. 2). In the foregoing case, the net force $u - F$ does not have a high magnitude in the negative direction just before the increase of the input in the positive direction. On the other hand, in all of the time intervals with gradual transitions, the initial value of the net force $u - F$ is a *high* value in the opposite direction to the oncoming direction of the input change.

3 Development of a Friction Model

In this section, we propose a friction model to capture the friction phenomena mentioned in Sec. 2. According to the free body diagram in Fig. 1(*b*), the constrained rigid beam dynamics can be described by the following equation:

$$I\ddot{\theta} = u - F - b\dot{\theta} - f \tag{2}$$

where I is the a constant proportional to the moment of inertia, b is the overall damping parameter, and the reaction end-point force F is described as $F = K\theta$. The experimental observations in Fig. 2 reveal that the gradual transitions occur only when the net force has been high enough in the opposite direction just

[1]Assuming F is linearly proportional to θ, as the encoder indicates no deflections, in the last 2.4 sec in Fig. 2, which is the steepest portion for F, the magnitude of mean angular velocity should be less that $0.072\ \text{deg}/2.4\ \text{s} = 0.03\ \text{deg}\,\text{s}^{-1}$.

[2]The dotted graph is obtained by inspection and assuming that the magnitudes of breakaway level and Coulomb friction are equal, the same in opposite directions of rotation, and dependent on the applied force F during the major rising or falling modes. Because of the slow motion, at each instant of time in Fig. 2, the actual friction force f is equal to $u - F$, with F representing the force measured by the force sensor (the thick solid line). In the first major rising mode in Fig. 2 ($t \in [21,30]$ s), the beam is slowly rotating in the positive direction and the friction force is equal to its upper threshold value, denoted by F_c^+, which increases almost linearly with the applied force. Hence, during the foregoing time interval, an ordinary friction model, with its upper threshold value depending on the applied force (equal to the measured values of f in Fig. 2 in the interval of $t \in [21,30]$ s), should predict an end point force similar to the measured one. As the actuation input stops increasing after $t = 30$ s, the beam rapidly enters into a standstill period during which the end point force remains constant. Based on an ordinary friction model, the standstill period lasts until the actuation input either decreases enough to bring the friction force to the lower threshold value $-F_c^-$, or increases to bring the friction again to the upper threshold. The latter happens first at $t = 36$ s, which justifies the horizontal dotted line during $t \in [30,36]$ s. The reasoning to justify the rest of the dotted graph in Fig. 2 is similar.

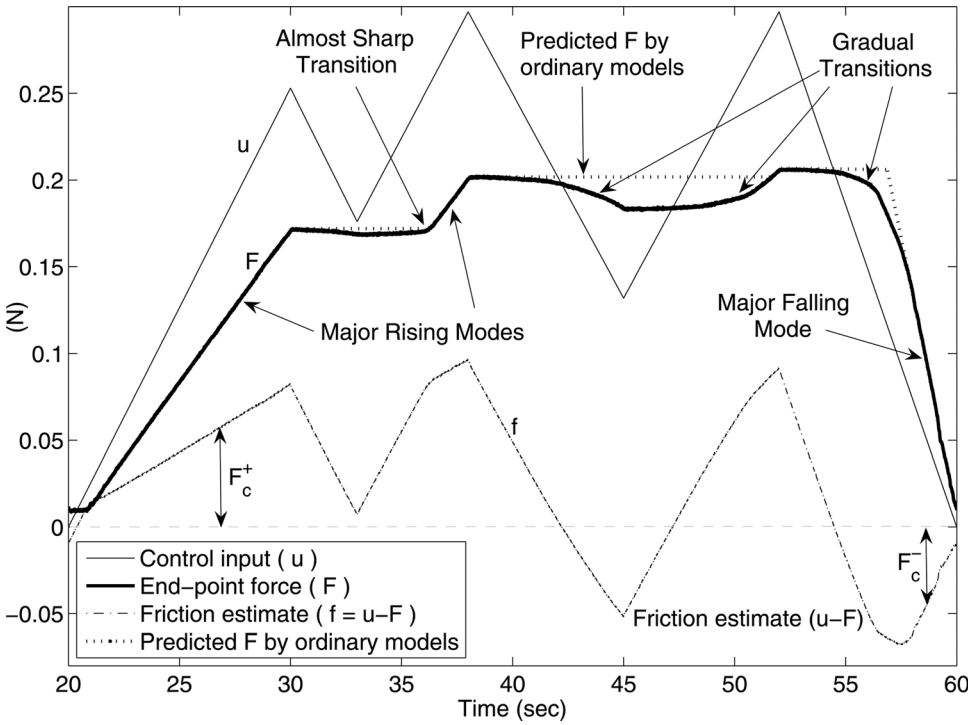

Fig. 2 Open-loop low-frequency response of the end-point force *F* (thick solid line) to a slowly varying control input *u* (thin solid), along with the estimation of friction term $f \simeq u - F$ (dash-dot) and predicted end-point force values by ordinary models (dotted)

before the net force magnitude increases; otherwise no significant gradual transition is observed. To incorporate this hysteresis effect into a friction model, we consider history of the net-force $u-F$ and its time rate to incorporate appropriate and slight deviation of the friction term f from the net force $u-F$. To this end, from the hysteresis diagram shown in Fig. 4(*a*), the following model is obtained:

$$f = \begin{cases} \mathrm{Sat}_{L(F)}\left[k(v)L(F)\tanh\left(\dfrac{u-F}{k(v)L(F)}\right)\right], & \text{if: } Q=1 \\ \mathrm{Sat}_{L(F)}(u-F), & \text{Otherwise} \end{cases} \tag{3}$$

where Q is a logic signal which is high when the net-force $u-F$ has been highly in the opposite direction just before its magnitude

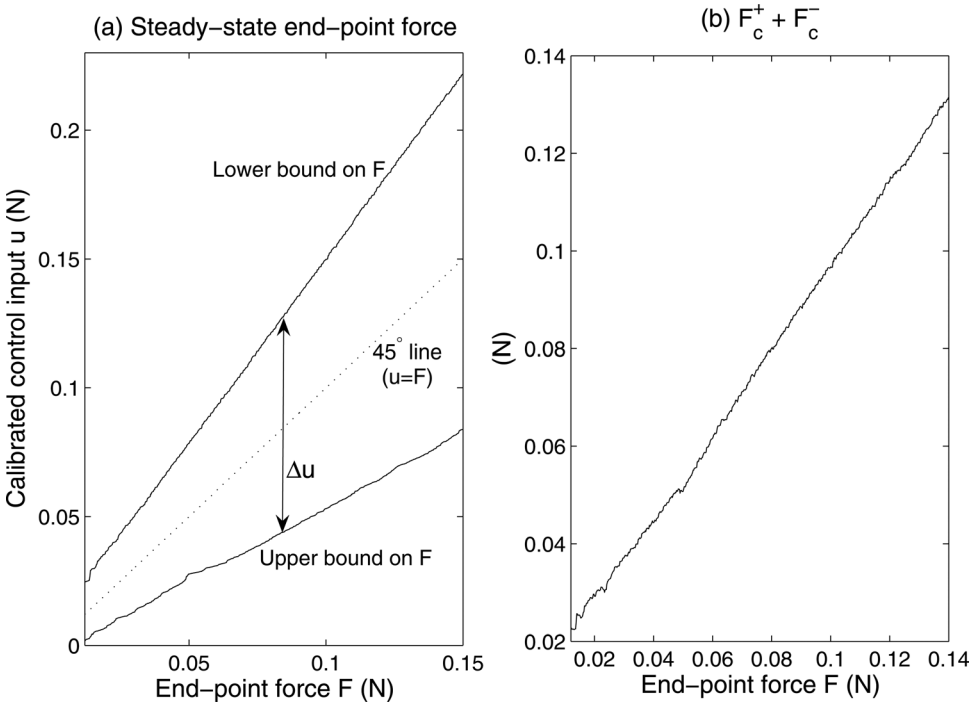

Fig. 3 (*a*) Maximum and minimum achievable end-point forces in steady-state with the rigid link and (*b*) estimated friction force interval $F_c^+ + F_c^-$ in terms of end-point force *F*

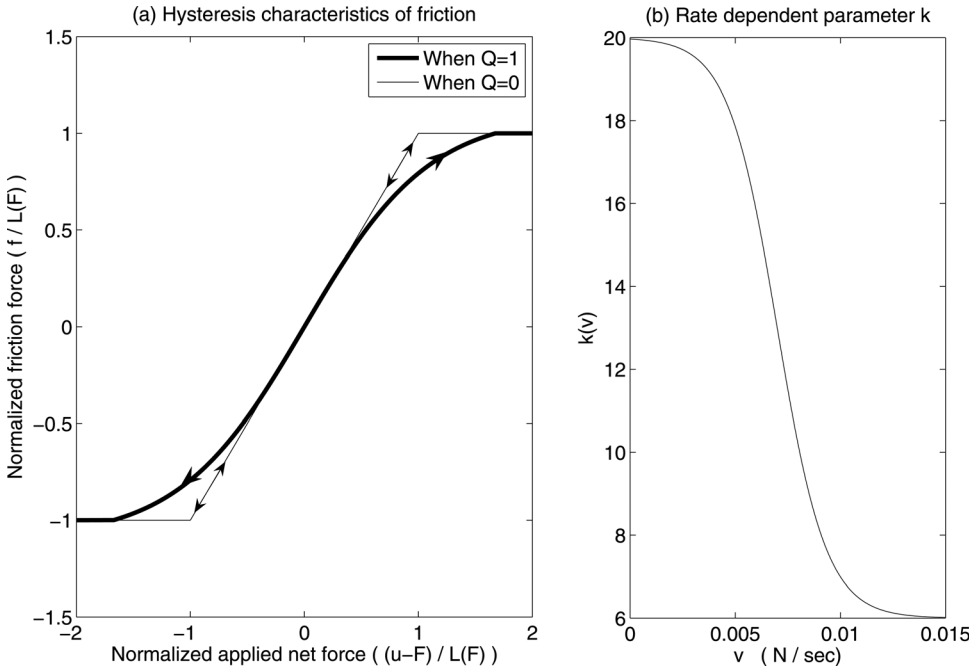

Fig. 4 (*a*) Diagram of friction model (3) for $k = 1.1$ and (*b*) dependency of parameter k on the net-force rate

starts rising, $L(F)$ is the maximum magnitude of friction while the end-point force F is applied, and functions $\mathrm{Sat}_L(\cdot)$ and $k(v)$ are defined in the following forms:

$$\mathrm{Sat}_L(x) = \begin{cases} x, & |x| < L \\ L\mathrm{sign}(x), & |x| \geq L \end{cases} \tag{4}$$

$$k(v) = \frac{k_{\max} + k_{\min}}{2} - \frac{k_{\max} - k_{\min}}{2} \tanh\left[M\left(\frac{v}{v_0} - 1\right)\right] \tag{5}$$

where the modeling parameters $k_{\max}$, $k_{\min}$, M, and v_0 determine the shape of the function with the net-force rate v is defined as follows:

$$v := \frac{d|u - F|}{dt} \tag{6}$$

A step-by-step logical sequence that leads to the foregoing force-based low-speed friction model can be presented as follows:

(1) $f = u - F$: This simple law leads to dynamic equation $I\ddot{\theta} + b\dot{\theta} = 0$, which does not depend on the actuation. Moreover, it predicts the invalid friction forces greater than the threshold values when magnitude of net force $u - F$ exceeds the breakaway values of friction.
(2) $f = \mathrm{Sat}_{L(F)}(u - F)$: The saturation function limits the predicted friction values within the threshold limits and resolves the problem in step 1. This friction law also includes the force dependency of threshold values by an appropriately shaped function $L(F)$. However, it cannot predict the hysteresis effect depicted by the gradual transitions in Fig. 2.
(3) $f = \mathrm{Sat}_{L(F)}\left[kL(F)\tanh\left(\frac{u-F}{kL(F)}\right)\right]$ with constant k: This friction law can predict the foregoing hysteresis effect. However, the gradual transitions happen irrespective of the history of the net force before the major rising or falling modes. Moreover, the model predicts excessive applied force values for low rate actuation inputs, as described in Fig. 7.
(4) f defined by Eq. (3) with $k(v)$ replaced by a constant k: The switching mechanism in the friction model fixes the first shortcoming of step 3, but the second one still remains to be solved.
(5) f defined by Eq. (3): The last shortcoming, regarding the prediction of excessive forces at very low rate inputs, is resolved by considering an appropriately defined function $k(v)$, which depends on the rate of magnitude of net force.

Dependency of parameter k on the net-force rate v with the following parameter values is shown in Fig. 4(*b*)

$$k_{\max} = 20,\ k_{\min} = 6,\ M = 3,\ v_0 = 0.007\frac{\mathrm{N}}{\mathrm{s}} \tag{7}$$

This rate dependency allows the gap between the thick and thin curves in Fig. 4(*a*) to decrease at low net-force rates, which causes less deviation of the friction term from the net force in slower speeds (see Sec. 3.1 for more details).

To design the logic signal, we use a combination of logic gates and relays with variable switching levels, given by

$$Q = (v > 0) \wedge \{[(u - F > 0) \wedge Q_2] \vee [(u - F < 0) \wedge Q_1]\} \tag{8}$$

where Q_2 and Q_1 are the outputs of the relays with characteristics as shown in Fig. 5 (*a*) and (b), respectively.

The relay output Q_2 goes high/low only when the net force $u - F$ crosses the switching level $-L_1/L_2$, while it is increasing/decreasing, respectively. Since we assumed that the friction exhibits symmetrical behaviors in different directions, the characteristics of the two relays are symmetrical when compared two each other. However, the model can be readily tailored to non-symmetrical friction behavior because the switching levels of the two relays can be selected independently. For the relay outputs to affect friction characteristics, the switching levels L_1 and L_2 should be lower than the maximum friction magnitude $L(F)$. The following values, which were identified by some experiments on the beam in constrained and unconstrained conditions, were used for the switching levels and other parameters

$$L_1 = 0.75L(F), \quad L_2 = 0.8L(F) \tag{9}$$

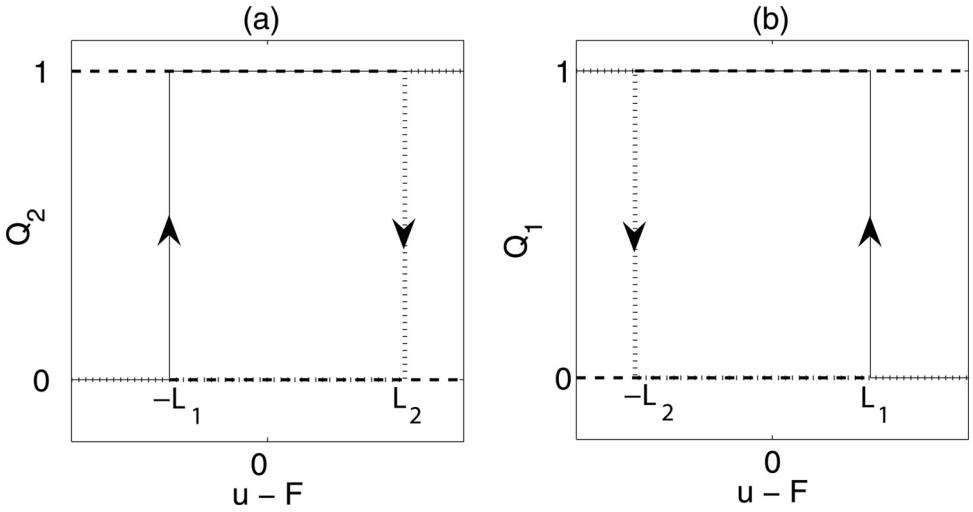

Fig. 5 Relay characteristics

$$I = 1.2 \times 10^{-4} \frac{Ns^2}{\text{deg}}, \quad b = 0.0288 \frac{Ns}{\text{deg}},$$
$$K = 3.84 \frac{N}{\text{deg}}, \quad L = 0.007 + 0.3|F| \ (N) \tag{10}$$

Simulation results of the end-point force predicted by the proposed method, and the above parameter values are shown in Fig. 6 (solid line). The results indicate that end-force exhibits a gradual/sharp transition to the major rising mode when the input has been deeply/shallowly below the applied force, which corresponds to the experimental results obtained in Sec. 2.

3.1 Justification of Friction Model Components. In this section, we provide justifications for different components in the proposed friction model. The saturation function in Eq. (3) is used to limit the predicted friction force to its maximum value determined by Coulomb or breakaway values. However, using just a saturation function in the following form:

$$f = \text{Sat}_{L(F)}(u - F) \tag{11}$$

for the friction model without considering any hysteresis effect leads to sharp transitions in the end-point force response as shown by the thin solid line in Fig. 7. Some of these sharp transitions agree with the experimental observations in Fig. 2, where the end-point force stops changing due to stiction for a time interval, which begins almost at the same time that the input rate is switched. This stopping behavior is almost as sharp as the input rate reversal. The end-point force then experiences a smooth gradual change before starting to change drastically (see Fig. 2). This smooth and gradual change in the end-point force, which is more significant at higher applied forces, cannot be predicted by the friction model (11), but the sharp stopping of the force is modeled with good accuracy (see the thin solid line in Fig. 7). A remedy to this problem is to increase the friction force magnitude more slowly than what is predicted by Eq. (11) as the net force applied to the hub rises in the stiction phase, but keeping model (11) when the net force magnitude is reduced. This idea is realized by

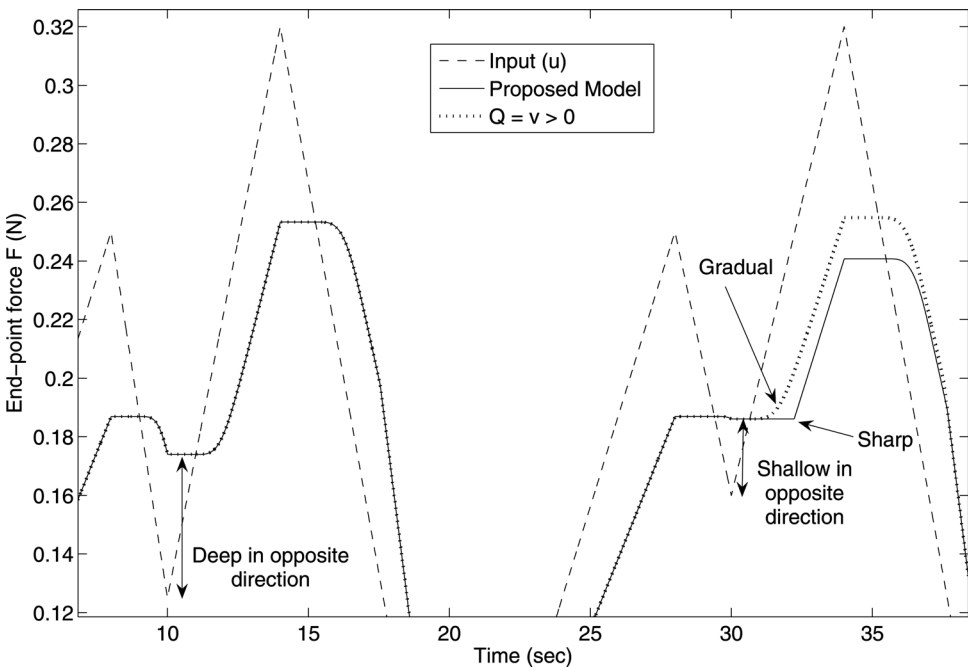

Fig. 6 Simulation results of the friction model with the proposed relays and without them

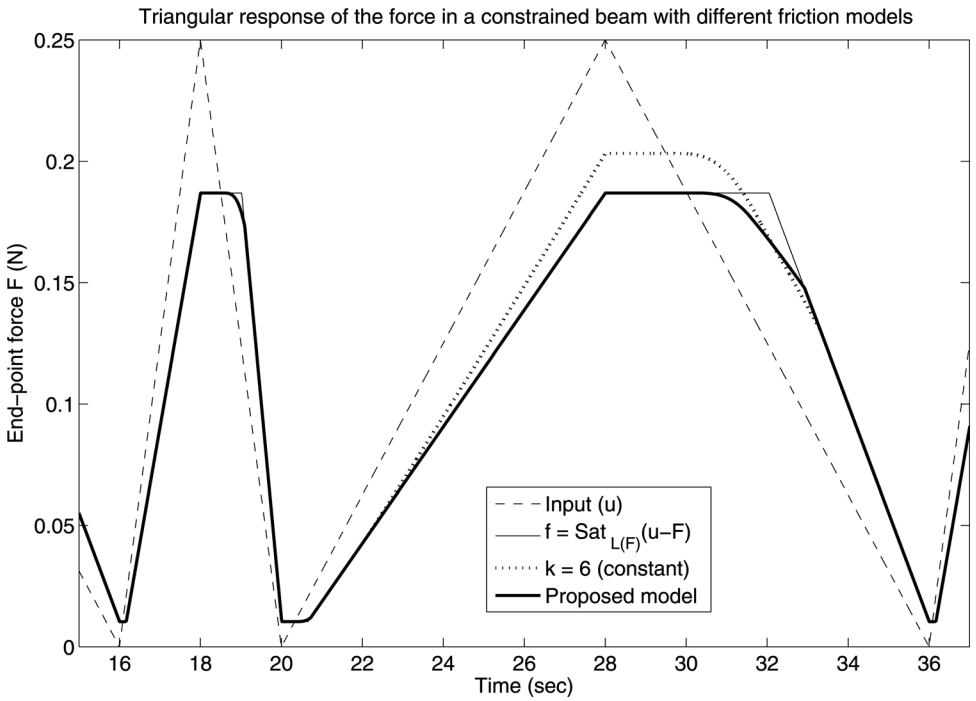

Fig. 7 Effect of hysteresis and rate-dependent *k* parameter

splitting the friction model expression as in the right hand side of Eq. (3), which leads to the hysteresis curve shown in Fig. 4.

The gap between the two curves in the hysteresis diagram can be reduced by increasing the values of k in (3) and vice versa. We assume that k depends on the net-force rate value v as in Eq. (5) and Fig. 4(*b*). If we select a constant value for k, e.g., $k = 6$, we may obtain inconsistent simulation results such as those shown in Fig. 7 with the dotted line, where the end-point force reaches a higher value with a more slowly increasing input. The reason for this inconsistency is that when the net-force $u - F$ changes more slowly, it may spend more time in the region where there is a gap between the curves in the friction hysteresis characteristics (Fig. 4(*a*)). A remedy to the foregoing problem is to reduce the gap when the magnitude of the net-force increases with a sufficiently low rate. By appropriate selection of function $k(v)$, which depends on the net-force rate, (Fig. 4(*b*)), the problem can be resolved significantly as shown by the thick solid line in Fig. 7.

The switching logic signal Q, which controls the switching between the hysteresis curves, is selected according to Eq. (8) to prevent any gradual transition in the end-point force response

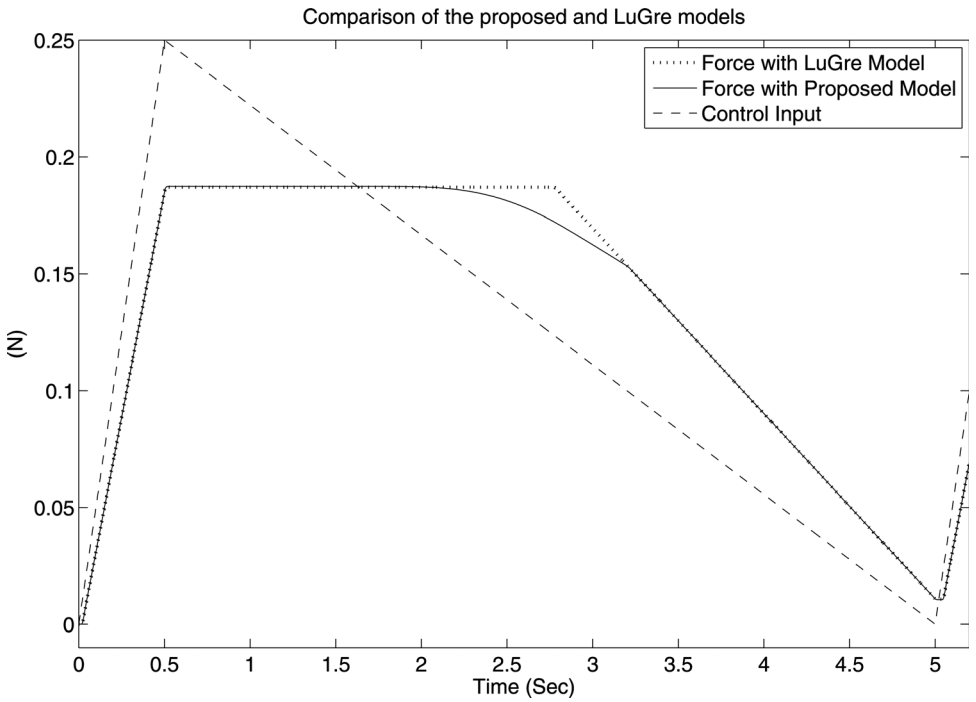

Fig. 8 Examination of the LuGre friction model in predicting the hysteresis behavior of friction and comparison with the proposed friction model

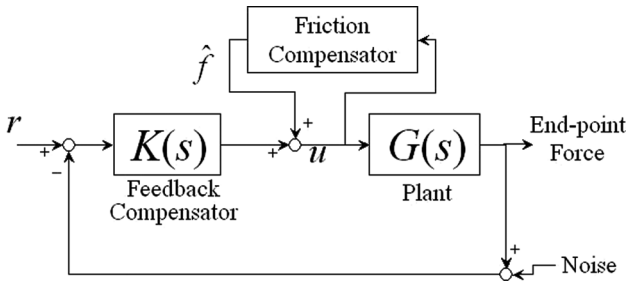

Fig. 9 Schematic diagram of the control system

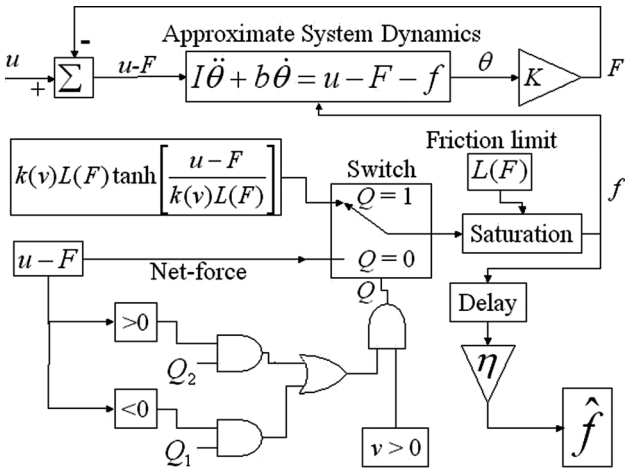

Fig. 11 Details of the friction compensator block in Fig. 9

when net force magnitude is going to increase without being deeply in the opposite direction. If we ignore the relay outputs Q_1 and Q_2, respectively, and simply consider $Q=v>0$, the gradual transitions would happen irrespective of starting from the deep or shallow points (dotted lines in Fig. 6) which do not agree with the experimental results.

4 A comparison With the LuGre Friction Model

In this section, the LuGre friction model is used to predict the end-point force F in the constrained arm. According to Ref. [15], the friction model is described by the following equation:

$$f_L=\sigma_0 z+\sigma_1\dot{z}+\sigma_2\omega,\quad \dot{z}=\omega-\frac{\sigma_0 z|\omega|}{F_C+(F_S-F_C)e^{-(\omega/\omega_s)^2}} \tag{12}$$

where $\omega=\dot{\theta}$, F_C is the Coulomb friction level, and F_S is the breakaway value. The friction force f_L given by Eq. (12) is used instead of f in the system dynamics (2), with $F_C=F_S=0.007+0.3|F|$ (N), $\sigma_0=10^5\,\frac{\text{N}}{\text{deg}}$, $\sigma_1=10^{2.5}\,\frac{\text{Ns}}{\text{deg}}$, $\sigma_2=0.4\,\frac{\text{Ns}}{\text{deg}}$, $I=1.2\times10^{-4}\,\frac{\text{Ns}^2}{\text{deg}}$. A sawtooth input is then applied to the system. The result is shown in Fig. 8 along with the result corresponding to the proposed model using parameter values of Eqs. (10) and (7). In both simulations, the friction force has been saturated between the force dependent breakaway values. Clearly, the LuGre model does not exhibit the hysteresis phenomenon as explained in Sec. 2 while the proposed model does, as demonstrated by the gap between the predicted end-point forces. Moreover, the simulation time taken by the LuGre model was found to be much longer than that of the proposed model, especially during the stiction. The reason is that the LuGre model is a velocity-based friction model, which uses the same continuous time differential equation for both sliding and stiction regimes, while the proposed model is a force-based friction model, which uses the net-force-rate instead of velocity and does not get stuck into the fast sign changes of the velocity during the stiction regime. Hence, the proposed model has the advantage of being implemented as an online friction identification scheme.

5 Application to Force Control

In this section, the proposed friction model is used for friction compensation in a force feedback control system as shown in Fig. 9. To identify the plant transfer function in Fig. 9, we applied a

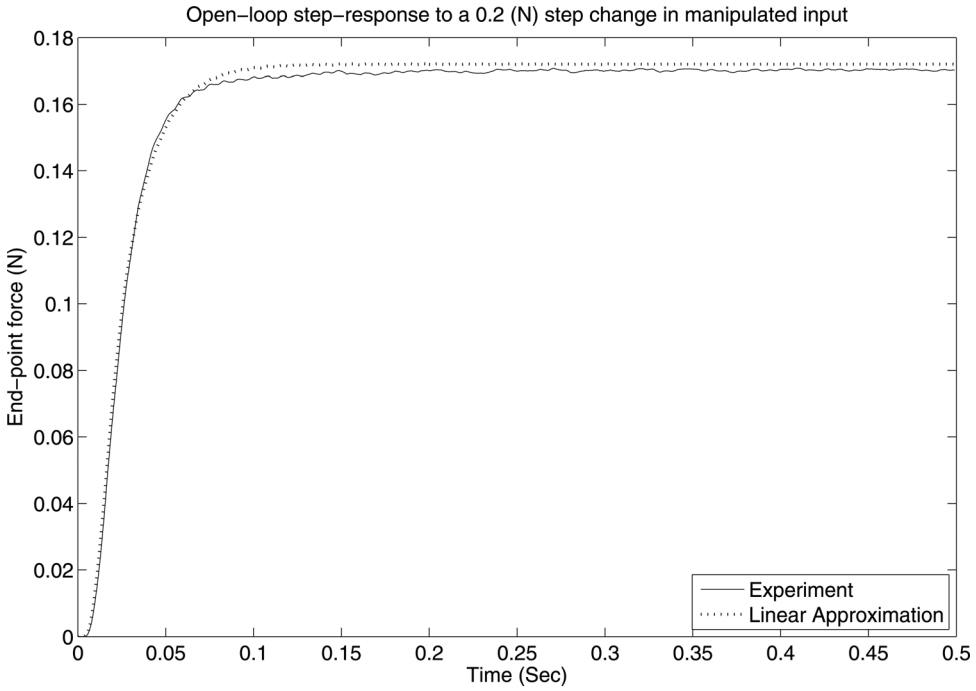

Fig. 10 Typical open-loop step-response of the end-point force and its approximation

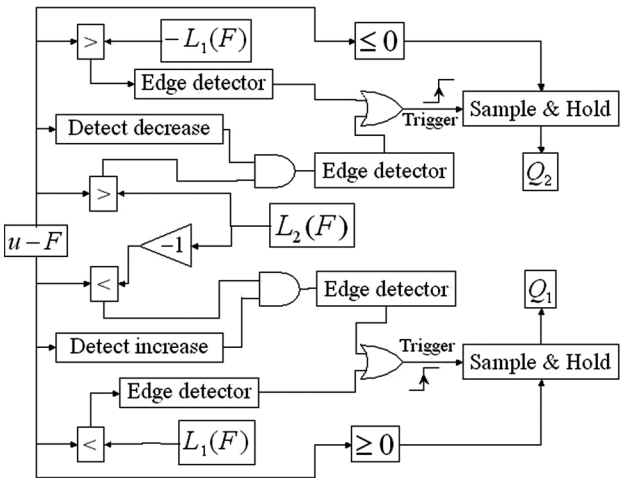

Fig. 12 Realization of the relay outputs Q_1 and Q_2 used in Fig. 11

step change 0.2 N to the scaled manipulated input. After shifting the starting point to the origin, the resulting open-loop step response of the end-point force along with a linear approximation is shown in Fig. 10. The approximate plant transfer function can be described by a steady-state gain 0.86, no zeros, and poles at $s=-55,-200,-139\pm203$, and $-5\pm778\,\frac{\text{rad}}{\text{s}}$. We used H_∞ mixed-sensitivity loop-shaping method to obtain compensator $K(s)$ as a robust optimal controller ("mixsyn" in MATLAB). In this method, the solution of the following problem determines the stabilizing compensator $K(s)$ such that the infinite norm of a vector composed of weighted closed-loop transfer functions is minimized [27,28]

$$\min_{K(s)} \| [w_p S, w_u K(s) S, w_T T] \|_\infty \tag{13}$$

where $S(s)=(1+GK)^{-1}$ and $T(s)=1-S(s)$ are sensitivity and complementary sensitivity functions, respectively, and weights $w_p(s)$, $w_u(s)$, and $w_T(s)$ are assigned by the designer and we selected them as

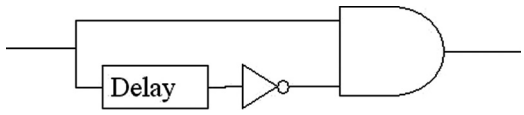

Fig. 13 Details of the edge detectors used in Fig. 12

$$w_p(s)=\frac{\frac{s}{1.1}+20}{s+20\times10^{-4}},\quad w_u=1,\quad w_T(s)=\frac{s+18.2}{10^{-4}s+20} \tag{14}$$

The feedback signal $\hat{f}$ provided by the friction compensator block in Fig. 9 is used to cancel the inherent friction of the plant, leaving an almost linear system as seen by the compensator $K(s)$. The structure of friction compensator, shown in Fig. 11 with more details, and its parameter values are similar to those mentioned Sec. 3. In this figure, the blocks indicated by ">0" and "<0" output high logic signals only when their inputs are positive and negative, respectively. Also, the upper input to the saturation block determines the limiting value of the predicted friction. Although an encoder at the hub can detect angular displacements up to 0.072 deg, no displacement was seen during the experiments because of the high stiffness of the stationary environment. Since the force sensor output is noisy, it is not suitable to be used in the force-rate-dependent Eqs. (3), (5), and (8). Hence, we incorporated the dynamic Eq. (2) into the friction compensator block of the control system as shown in Fig. 11. In this way, the end-point force which is used for friction estimation is calculated by $K\theta$, where θ is obtained by the state of the friction model. To prevent any algebraic loop, we incorporated a small time delay in the friction block. The predicted friction force is weakened by a positive coefficient $\eta=0.85$ to prevent overcompensation. Realizations of the relay outputs Q_1 and Q_2 are shown in Fig. 12, where the double input blocks indicated by "$>$" or "$<$" output high logic signals only when the left side input is more or less than the right side input, respectively, and the "Detect increase"/"Detect decrease" block's output is high when its input is rising/falling. The edge detector blocks, which produce a narrow pulse only on rising edges of their input, were realized by the logic circuit as shown in Fig. 13, where the width of the pulse, set by the incorporated delay, is 3 ms. The sample and hold blocks in Fig. 12 operate on

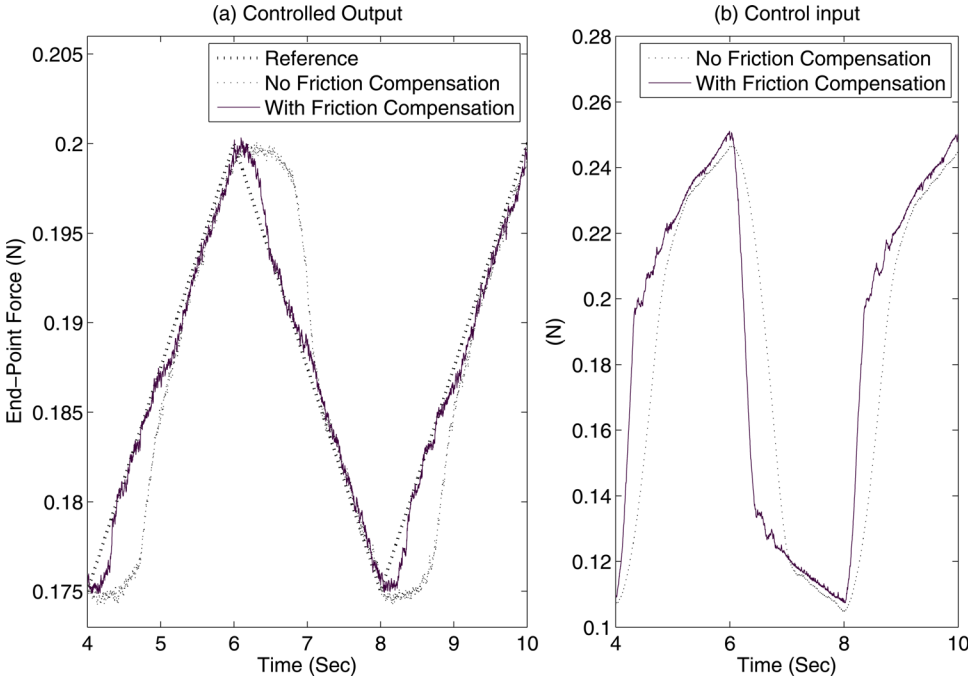

Fig. 14 Experimental results of friction compensation by the proposed model

the rising edge of the trigger input. Switching of the relay output Q_2/Q_1 to the low level, designed by the circuit in Fig. 12, may occur at net-force values larger/lower than $L_2/-L_2$. Hence, the downward arrows in Figs. 5(*a*) and 5(*b*) indicate, respectively, the minimum and the maximum level at which the corresponding relay output may switch to a low logic signal.

After discretizing the feedback and the friction compensators with a sampling time 1 ms, the feedback control system was examined for tracking of a triangular reference once with the friction compensation and another time without the friction compensation (i.e. $\eta = 0$). The experimental results, shown in Fig. 14, demonstrate that the proposed friction model is useful to reduce the tracking error in force control applications. Without friction compensation, the rms value of the steady-state force error is 0.0038 N while after friction compensation it is reduced to 0.001 N, which is considerably lower.

6 Conclusion

In this paper, based on the experimental observations, we studied friction characteristics of low-speed constrained arms. We observed two phenomena which should be considered in the friction models of the arms that interact with environments. The first one is that the breakaway level increases with the force applied by the arm. The second one is a hysteresis behavior during stiction, which makes the friction force increase more slowly than the external net force when the net force increases after a sufficient direction change. We offered a new friction model, which includes the described phenomena, which was verified by simulation and experiments. Application of the proposed model in friction compensation was also investigated in a robust feedback control system.

References

[1] Armstrong-Hélouvry, B., Dupont, P., and Canudas De Wit, C., 1994, "A Survey of Models, Analysis Tools and Compensation Methods for the Control Of Machines With Friction," Automatica, **30**(7), pp. 1083–1138.

[2] Armstrong-Hélouvry, B., *Control of Machines With Friction* (Academic Publishers, Kluwer, 1991).

[3] Feeny B., Guran, A., Hinrichs, N., and Popp, K., 1998, "A Historical Review on dry Friction and Stick-Slip Phenomena," Appl. Mech. Rev., **51**(5), pp. 321–341.

[4] Ni, J., and Zhu, Z., 2001, "Experimental Study of Tangential Micro Deflection of Interface of Machined Surfaces," ASME J. Manuf. Sci. Eng., **123**(2), pp. 365–367.

[5] Olsson, H., Åström, K. J., Canudas de Wit, C., Gäfvert, M., and Lischinsky, P., 1998, "Friction Models and Friction Compensation," Eur. J. Control, **4**(3), pp. 176–195.

[6] Karnopp, D., 1985, "Computer Simulation of Slip-Stick Friction in Mechanical Dynamic Systems," ASME J. Dyn. Syst., Meas., Control, **107**(1), pp. 100–103,

[7] Dahl, P. R., 1968, "A Solid Friction Model," Technical Report No. TOR-0158(3107-18)-1, The Aerospace Corporation, El Segundo, CA.

[8] Dahl, P. R. 1976, "Solid Friction Damping of Mechanical Vibrations," AIAA J., **14**(12), pp. 1675–1682.

[9] Haessig, D. A., and Friedland, B., 1991, "On the Modeling and Simulation of Friction," ASME J. Dyn. Syst., Meas., Control, **113**(3), pp. 354–362.

[10] Bliman, P.-A., and Sorine, M., 1991, "Friction Modelling by Hysteresis Operators: Application to Dahl, stiction, and Stribeck effects," *Proceedings of the Conference on Models of Hysteresis*, Trento, Italy, pp. 10–19.

[11] Bliman, P.-A., and Sorine, M., 1993, "A system-theoretic Approach of Systems With Hystereis: Application to Friction Modelling and Compensation," *Proceedings of the second European Control Conference*, Groningen, The Netherlands, pp. 1844–1849.

[12] Bliman, P.-A., and Sorine, M., 1995, "Easy-to-use Realistic Dry Friction Models for Automatic Control," *3rd European Control Conference*, Rome, Italy, pp. 3788–3794.

[13] Harnoy, A., and Friedland, B., 1994, "Dynamic Friction Model of Lubricated Surfaces for Precise Motion Control," Tribol. Trans., **37**(3), pp. 608–614.

[14] Harnoy, A., and Friedland B., 1994, "Modeling and simulation of Elastic and Friction Forces in Lubricated Bearings for Precise Motion Control," Wear, **172**, pp. 155–165.

[15] Canudas de Wit, C., Olsson, H., Åström, K. J., and Lischinsky, P., 1995, "A New Model for Control of Systems With Friction," IEEE Trans. Autom. Control, **40**(3), pp. 419–425.

[16] Dupont, P., Armstrong, B., and Hayward, V., 2000, "Elasto-plastic Friction Model: Contact Compliance and Stiction," Proceedings of the American Control Conference, **2**, pp. 1072–1077.

[17] Dupont, P., Hayward, V., Armstrong, B., and Altpeter, F., 2002, "Single State Elastoplastic Friction Models," IEEE Transactions on Automatic Control, **47**(5), pp. 787–792.

[18] Swevers, J., Al-Bender, F., Ganseman, C. G., and Projogo, T., 2000, "An Integrated Friction Model Structure With Improved Presliding Behavior for Accurate Friction Compensation," IEEE Trans. Autom. Control, **45**(4), pp. 675–686.

[19] Lampaert, V., Swevers, J., and Al-Bender, F., 2002, "Modification of the Leuven Integrated Friction Model Structure," IEEE Trans. Autom. Control, **47**(4), pp. 683–687.

[20] Al-Bender, F., Lampaert, V., and Swevers, J., 2004, "A Novel Generic Model at Asperity Level for Dry Friction Force Dynamics," Tribol. Lett., **16**(12), pp. 81–93.

[21] Al-Bender, F., Lampaert, V., and Swevers, J., 2005, "The Generalized Maxwell-slip Model: A Novel Model for Friction Simulation and Compensation," IEEE Trans. Autom. Control, **50**(11), pp. 1883–1887.

[22] Gonzalez, J. J., and Widmann, G. R., 1992, "Investigation of Nonlinearities in the Force Control of Real Robots," IEEE Trans. Syst. Man Cybern., **22**(5), pp. 1183–1193.

[23] Gonzalez, J. J., and Widmann, G. R., 1995, "A Force Commanded Impedance Control Scheme for Robots With Hard Nonlinearities," IEEE Trans. Control Syst. Technol., **3**(4), pp. 398–408.

[24] Gonzalez, J. J., and Widmann, G. R., 1997, "A New Model for Nonlinear Friction Compensation in the Force Control of Robot Manipulators," IEEE International Conference on Control Applications, pp. 201–203.

[25] Kwon, D. S., and. Woo, K. Y., 2000, "Control of the Haptic Interface With Friction Compensation and Its Performance Evaluation," IEEE/RSJ International Conference on Intelligent Robots and Systems, pp. 955–960.

[26] Bazaei, A., and Moallem, M., 2010, "Presticion Friction Modeling and Position Control in an Actuated Rotary Arm," IEEE Trans. Instrum. Meas. **59**(1), pp. 131–139.

[27] Skogestad, S., and Postlethwaite, I., 2005, *Multivariable Feedback Control, Analysis and Design*, 2nd ed., John Wiley & Sons, Chichester, England, pp. 62–65.

[28] Bazaei, A., and Moallem, M., 2009, "Force Transmission through a Structurally Flexible Beam: Dynamic Modeling and Feedback Control," IEEE Trans. Control Syst. Technol., **17**(5), pp. 1245–1256.